Journal of The Electrochemical Society, **165** (9) B370-B377 (2018)
0013-4651/2018/165(9)/B370/8/$37.00 © The Electrochemical Society

Determination of Neurotransmitter in Biological and Drug Samples Using Gold Nanorods Decorated *f*-MWCNTs Modified Electrode

Mani Govindasamy,[1] Shaktivel Manavalan,[1] Shen-Ming Chen,[1,2,*,z] Umamaheswari Rajaji,[1] Tse-Wei Chen,[1,3] Fahad M. A. Al-Hemaid,[2] M. Ajmal Ali,[2] and Mohamed Soliman Elshikh[2]

[1] *Department of Chemical Engineering and Biotechnology, National Taipei University of Technology, Taipei 106, Taiwan*
[2] *Department of Botany and Microbiology, College of Science, King Saud University, Riyadh 11451, Saudi Arabia*
[3] *Research and Development Center for Smart Textile Technology, National Taipei University of Technology, Taipei, Taiwan*

We described a nanocomposite material that consists of gold nanorods self-assembled on functionalized multiwalled-carbon nanotubes (Au NRs@*f*-MWCNTs). It was deposited on a screen-printed carbon electrode (SPCE) which then is well suited for sensitive and selective determination of dopamine. Au NRs are prepared by silver ion-assisted seed-mediated method and the Au NRs@f-MWCNTs was prepared by self-assembly of Au NRs on *f*-MWCNTs. The composite was characterized by X-ray diffraction, transmission electron microscopy, Raman, UV-visible, and energy-dispersive X-ray spectroscopy. The electrochemical analyses were carried out using inexpensive SPCE to modify nanocomposite and visualized signals by cyclic voltammetry and amperometric instrument. The electrode displays excellent electrocatalytic ability to catalyze the redox reaction of dopamine. The modified SPCE, best operated at a working potential as low as 0.12 V (vs. Ag/AgCl), responds linearly to dopamine in the 3.5 nM to 1550 μM concentration range. The detection limit is 5.0×10^{-10} (±0.82) M, and the sensitivity is 4.04 (±0.58) $\mu A.\mu M^{-1}.cm^{-2}$. The limit of quantification (LOQ) of the method was 16.6×10^{-10} (±1.2) M. The sensor has good selectivity, appreciable stability, and reproducibility. It was applied to the determination of dopamine in (spiked) human serum and rat brain samples.
 [DOI: 10.1149/2.1351809jes]

Manuscript submitted April 16, 2018; revised manuscript received May 25, 2018. Published June 22, 2018.

Dopamine (DA) is a neurotransmitter in mammalian central nervous systems that plays a central role in the brain reward system.[1] It controls arousal and motivation and regulates movements and coordination of the body. The DA dysregulation is directly liked to several behavioral disorders such as addiction, memory loss, depression, and loss in coordination.[2,3] The inability of the neural cells to produce sufficient DA leads to life-threating neurological disorders such as, Parkinson's disease, and schizophrenia.[4] Therefore, the development of reliable DA sensing methods is highly important.[5] To date, a variety of analytical methods such as chromatography, capillary electrophoresis, chemiluminescence, and spectroscopy have been employed for DA quantification, however many of the them are expensive, laborious and bulky[5] Taking advantage of exceptional traits, such as being easy-to-operate, fast response time, low-cost, portable, sensitive, and simple-to-fabricate, electrochemical techniques are preferably suitable to the determination of DA. Electrochemical DA sensing at unmodified electrodes encounter poor selectivity, low sensitivity, surface fouling, and lack of reproducibity.[6] Nanomaterials modified electrodes are promising probes to circumvent the aforementioned analytical issues owing to their large unique surface properties.[7–9] In view of that, the preparation of robust nanocomposite materials for electrocatalytic DA sensing is of great interest for practical applications.

Multi-walled carbon nanotubes (MWCNTs) have extraordinary physico-chemical properties and widely used electrode material in electroanalytical chemistry.[10,11] Nevertheless, pristine MWCNTs alone are unable to produce aqueous processable.[12,13] The installation of oxygen functionalities on the surface of MWCNTs produces functionalized MWCNTs (*f*-MWCNTs), which are processable in aqueous solutions. Due to the presence of abundant functional groups and delocalized π bonding, *f*-MWCNTs are suitable supports to anchor metal/metal oxide nanostructures.[14,15] Gold (Au) nanostructures are the most investigated metal nanostructures in analytical chemistry owing to their extraordinary electrocatalytic, electronic and optical properties. MWCNTs are suitable supports to stabilize nano sized Au particles.[16,17] Because, the morphology has significant impact on the performance, controlled syntheses of nano Au to implement desired shape and size is important.[6] Different shapes of Au, including particles,[18] sheets,[19] spheres,[20] cubes,[21] flowers,[22] etc., have been reported in the previous methods. Among them, Gold nanorods (Au NRs) show high potential in electrochemical sensing owing to their excellent conductivity, enhanced surface area, electrocatalytic activity, selectivity and sensitivity.[23,24] A silver ion-assisted seed-mediated method can produce uniform sized active Au NRs.[25] By combining solution based self-assembly procedure and seed-mediated method, here we described a synthetical route to prepare Au NRs decorated *f*-MWCNTs (Au NRs@*f*-MWCNTs) for sensitive and selective electrochemical DA sensing applications. Both *f*-MWCNTs and Au NRs are separately prepared via acid-treatment and seed-mediated method, respectively. Subsequently, Au NRs are undergone self-assembly on the walls of *f*-MWCNTs through simple ultrasonic agitation. Electrostatic interaction between negatively charged surface of *f*-MWCNTs and positively charged surface of Au NRs stabilizes the resulting material. The Au NRs@*f*-MWCNTs modified screen-printed electrode displays excellent DA sensing ability not only in lab samples, but also in real samples.

Experimental

Chemicals and instrumentation.—The chemicals and instrumentation are described in the supplementary information.

Synthesis of Au NRs@f-MWCNTs nanocomposite.—The *f*-MWCNTs and Au NRs were prepared separately and then self-assembled through ultrasonic agitation to yield Au NRs@*f*-MWCNTs nanocomposite as described in Scheme 1. To prepare *f*-MWCNTs, 50 mg MWCNTs were added to a 100 mL mixture of H_2SO_4 and HNO_3 (3:1) and ultrasonicated for 3 h. After filtration and several washings (water and ethanol), the purified *f*-MWCNTs powder was obtained. The Au NRs were prepared through silver ion-assisted seed-mediated method by following reported procedure with little modification.[25] 0.5 mM aqueous solution of $HAuCl_4$ (10 mL) and 0.2 M aqueous solution of CTAB (10 mL) were added to beaker and mixed for 10 min via magnetic stirrer to yield a seed solution. Next, ice-cold aqueous solution of $NaBH_4$ (1 mL, 5 mM) was freshly prepared, added to the as-prepared Au(III)–CTAB seed solution and vigorously stirred for 5 min. The resulting CTAB-stabilized Au seed solution was kept aside for 1 h prior to its use. Next, the growth solution was prepared by mixing $AgNO_3$ (500 μL, 10 mM), $HAuCl_4$ (2 mL, 10 mM) and CTAB (50 mL, 0.1 M) in a beaker. Subsequently,

*Electrochemical Society Member.
[z]E-mail: smchen1957@gmail.com; smchen78@ms15.hinet.net

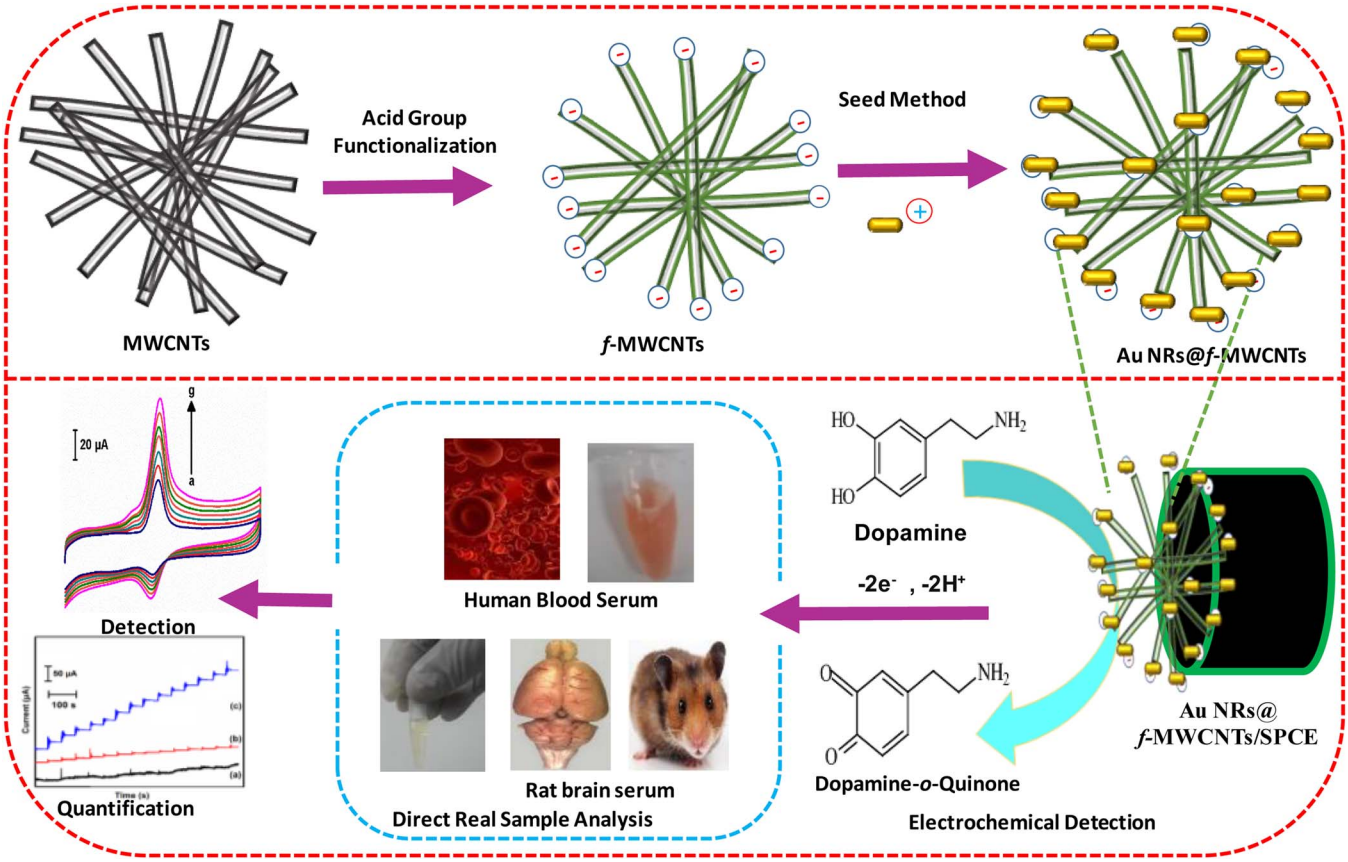

Scheme 1. Schematic representation for the synthesis of Au NRs decorated MWCNTs and its electrochemical sensing application.

1 mL of HCl and 10 mg of ascorbic acid were added successively and mixed for 15 min to obtain growth solution. Next, 10 mg of *f*-MWCNTs were added and stirred with magnetic stirrer for 30 min. To this solution, the CTAB-stabilized Au seed solution was added. Finally, the whole reaction mixture was kept aside for overnight to yield Au NRs@*f*-MWCNTs which was then separated, washed and freeze-dried. 0.5 mg mL^{-1} aqueous dispersion of Au NRs@*f*-MWCNTs was prepared and stored.

Fabrication of Au NRs@f-MWCNTs modified SPCE.—First, the working electrode surface of SPCE was pre-cleaned by potential cycling between −1.0 V and 1.2 V, in 0.1 M phosphate buffer (pH 7.0) for 5 cycles at a scan rate of 25 mV s^{-1}. About, 6 μL aqueous dispersion of Au NRs@*f*-MWCNTs was drop casted onto the pre-cleaned SPCE and dried at ambient conditions.

Preparation of real samples.—Rat brain and human serum samples were collected from Chang Gung University, Taiwan and the experimental protocol were approved by the Institutional Animal Ethics Committee. About 1 mL of rat brain and 1 mL of human serum samples were added to 10 mL of phosphate buffer (pH 7.0). The diluted samples are found to be DA free. Then, known amounts of DA were spiked and analyzed using GNR@*f*-MWCNTs modified electrode. Dopamine hydrochloride injection was obtained from a local medical hospital and used without any pre-treatment. The detection of DA was carried out by injecting aliquots of dopamine hydrochloride injection sample into phosphate buffer (pH 7.0).

Results and Discussion

Characterizations of Au NRs@f-MWCNTs.—Figure 1a displays the XRD patterns of *f*-MWCNTs and Au NRs@*f*-MWCNTs nanocomposite. The diffraction pattern of *f*-MWCNTs featured with a characteristic peak at 2θ of 26.3° indexed to (002) that can be correlated to graphitic structure.[26] The XRD pattern of Au NRs@*f*-MWCNTs featured with peaks at 27.3°, 38.6°, 44.68°, 64.68°, 77.96°, and 82.45° corresponding to the lattice planes of (002), (111), (200), (220), (311), and (222), respectively. The XRD pattern of Au NRs@*f*-MWCNTs is consistent with the characteristic pattern of Au metal (JCPDS file: 04-0784) as well as it included with the characteristic band of *f*-MWCNTs.[18] Raman spectroscopy can be used to obtain information about the degree of disorder in graphene materials. As shown in Figure 1b, the Raman spectra of MWCNTs (inset), *f*-MWCNTs (curve a), Au NRs@*f*-MWCNTs (curve b) display characteristic D and G bands. Generally, the defect density in sp^2 lattice of graphitic materials can be elucidated based on D band to G band intensity ratio (I_D/I_G).[27] Here, the value of I_D/I_G for MWCNTs, *f*-MWCNTs, and Au NRs@*f*-MWCNTs are found to be 0.23, 1.21, and 1.25. Expectedly, the I_D/I_G value of *f*-MWCNTs was 5.26-fold increase compared with pristine MWCNTs due to introduction of plenty of defects on during functionalization process. However, there is no significant difference in the I_D/I_G values of *f*-MWCNTs and Au NRs@*f*-MWCNTs, which indicates no structural changes during composite formation. The UV-Vis spectra of *f*-MWCNTs (curve a) and Au NRs@*f*-MWCNTs (curve b) are given as Figure 1c. Water is used as solvent to perform UV-vis spectroscopy experiments. No obvious peak was observed in the spectrum of *f*-MWCNTs. However, a distinctive sharp peak was obtained at 530 nm, which is a typical surface plasmon resonance band of Au NRs, thus confirms Au NRs.[28]

The HR-TEM image of *f*-MWCNTs displays a typical tube-like morphology (Figure 2a). The HR-TEM image of Au NRs@*f*-MWCNTs featured with the presence of both tubes as well as rods, where tubes can be related to *f*-MWCNTs and rods can be related to Au NRs. The Au NRs are non-aggregated and uniformly distributed on the networks of *f*-MWCNTs backbone (Figure 2b). It is well-known that the surface of *f*-MWCNTs is negatively charged

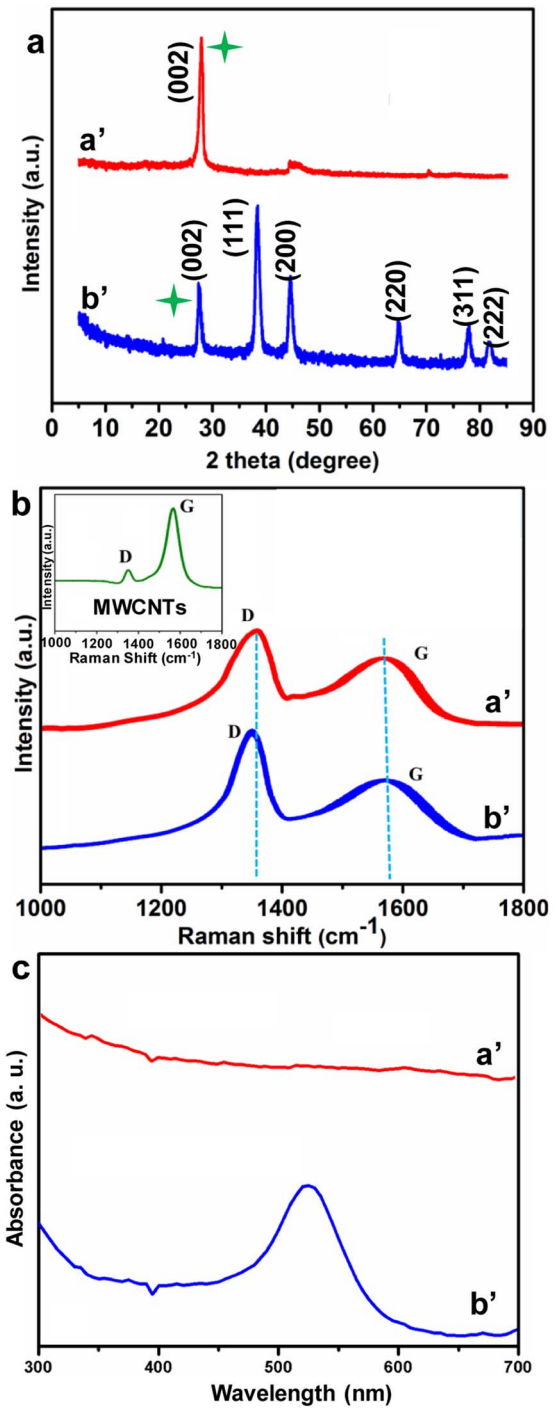

Figure 1. (a) XRD pattern, (b) Raman spectra, and (c) UV-visible spectra of *f*-MWCNTs (a') and Au NRs@*f*-MWCNTs (b'). Inset to Figure 1b: Raman spectrum of MWCNTs.

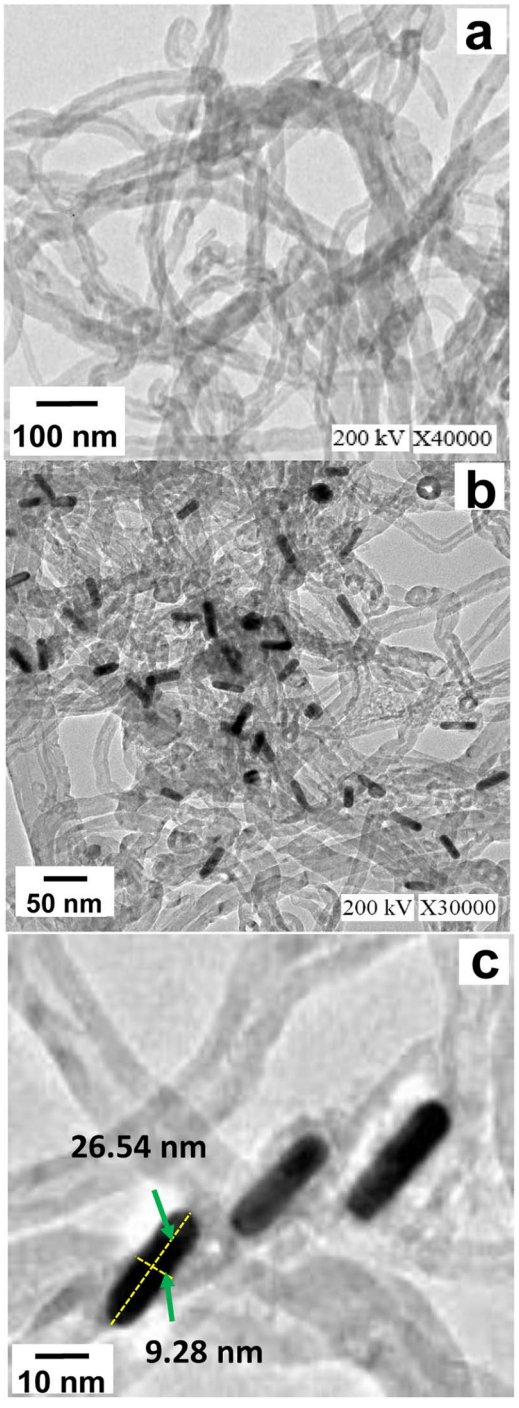

Figure 2. HR-TEM images of *f*-MWCNTs (a), and Au NRs@*f*-MWCNTs (b and c).

due to the presence of oxygen functionalities, while the surface of Au particles is positively charged.[29] Therefore, the self-assembly of Au NRs on *f*-MWCNTs is predicted to be highly favorable interaction in the composite through electrostatic interaction. Since the Au NRs contain a fraction of CTAB, it can assist immobilization of Au NRs on the basal plane of *f*-MWCNTs. From high magnification TEM image, average length and width of Au NRs are calculated to be 26.54 nm and 9.28 nm (Figure 2c). Thus, nanorod shaped gold particles are successfully formed on the surface of *f*-MWCNTs. The EDX profile of Au NRs@*f*-MWCNTs displays signals from expected elements C, O, and Au atoms with atomic percentages of 52.36% (±2.46), 27.52% (±1.42), and 20.12% (±1.70), respectively (Figure S1a). The presence of oxygen content is originated from the oxygen functionalities located on *f*-MWCNTs. The mapping of Au NRs@*f*-MWCNTs displayed the distribution of elements, wherein Au atom appeared as shell, while C and O atoms are appeared as core (Figure S1b-e).

The chemical states of the composite are evaluated by XPS studies (Figure 3). The survey scan (Figure 3a) shows the existence of graphitic C 1s peak at 283.5 eV, a weak O 1s peak at 530.5 eV, and a pronounced Au 4f peak at 82–89 eV. The XPS curve fitting of C 1s spectrum exhibits four peaks ranging from 282–290 eV as shown in Figure 3b. The major peak at 283.5 eV can be assigned to the sp^2 carbon atoms (C1) constituted graphitic regions, and its presence

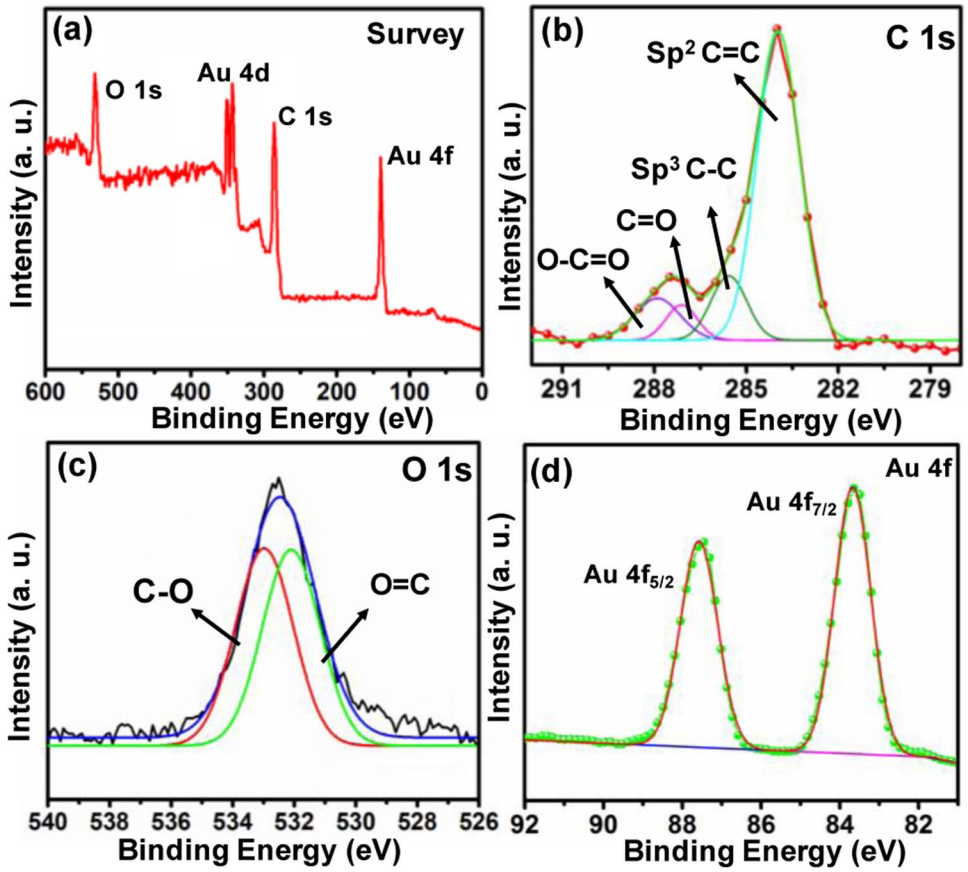

Figure 3. (a) XPS survey spectra of the Au NRs@*f*-MWCNTs; (b) C1s (c) O1s and (d) Au 4f.

indicates that most of the C atoms are arranged in a honeycomb lattice. The other three peaks at 286.4, 287.1 and 288.2 eV were corresponding to C–O, C=O, and O=C–O groups, respectively and the results are consistent previous report.[30] The O 1 s spectrum can be deconvoluted into two sub-peaks at 532.1 and 533.2 eV which can be correlated to C=O, and C–O respectively (Figure 3c).[30] The XPS spectrum of Au 4f core displays major peaks at 83.7 and 87.6 eV correspond to the binding energies of Au $4f_{7/2}$ and Au $4f_{5/2}$, respectively, and these peaks are characteristic peaks for metallic Au^0 (Figure 3d).[31] The XPS analysis is consistent with previous reports and indicates the successful formation of Au NRs@*f*-MWCNTs.

Electrochemical behavior of Au NRs@f-MWCNTs.—The impedance spectra were represented as Nyquist plots (EIS). The semicircle part at higher frequencies is related to electron transfer limited process and the linear part at lower frequency region is related to diffusion-limited process. Figure 4A shows the EIS curves obtained at bare SPCE (a), *f*-MWCNTs/SPCE (b), and Au NRs@*f*-MWCNTs/SPCE (c) modified electrodes in 0.1 M KCl containing 5 mM $Fe(CN)_6^{3-/4}$. The frequency range was 0.1 Hz to 1 MHz and the amplitude was 5 mV. Randles equivalent circuit model was used to fit the experimental data (inset to Figure 4A). The parameters are electrolyte resistance (R_s), charge transfer resistance (R_{ct}), double layer capacitance (C_{dl}) and Warburg impedance (Z_w), respectively.[32,33] The R_{ct} values obtained at bare SPCE, *f*-MWCNTs/SPCE, and Au NRs@*f*-MWCNTs/SPCE are 362.62 Ω, 173.35 Ω, and 64.26 Ω. The EIS result indicates resistance at Au NRs@*f*-MWCNTs/SPCE has been considerably reduced, which is ascribed to the excellent electronic conductivity property of Au NRs@*f*-MWCNTs composite.

The electrochemical behavior of bare SPCE (a), *f*-MWCNTs/SPCE (b) and Au NRs@*f*-MWCNTs/SPCE (c) was probed by cyclic voltammetry (Figure 4B). 0.1 M KCl was used as supporting electrolyte and 5 mM $[Fe(CN)_6]^{3-/4-}$ was used as redox probe. Compared to *f*-MWCNTs/SPCE, the Au NRs@*f*-MWCNTs/SPCE shows higher redox peak currents and smaller peak-to-peak potential separation. Figure S2, shows Au NRs@*f*-MWCNTs/SPCE toward $[Fe(CN)_6]^{3-/4-}$ at varied scan rates from 0.01–0.1 V s^{-1} and corresponding plot between peak current and square root of scan rate. The electrochemical active surface area of the modified electrode was assessed by substituting slope value of different scan rate plot in Randles–Sevcik Equation 1.[34]

$$i_p = 2.72^{*}10^5 n^{3/2} A D^{1/2} C \upsilon^{1/2} \quad [1]$$

Here, i_p is peak current, n is number of electrons involved in the redox reaction, transfer, υ is scan rate (Vs^{-1}), A is electrochemical active area (cm^2), D is the diffusion coefficient (cm^2 s^{-1}), C is the concentration of $[Fe(CN)_6]^{3-/4-}$ (mol cm^{-3}).[35] The electrochemically active surface areas were calculated to be 0.061, 0.127, and 0.215 cm^2 for bare SPCE, *f*-MWCNTs/SPCE, and Au NRs@*f*-MWCNTs/SPCE respectively. Thus, the active area of Au NRs@*f*-MWCNTs/SPCE is indicating that the nanocomposite is suitable for electrocatalytic sensing applications.

Electrocatalysis of dopamine at Au NRs@f-MWCNTs/SPCE.—Figure 5a shows the cyclic voltammograms obtained at unmodified SPCE (a'), *f*-MWCNTs/SPCE (b'), and Au NRs@*f*-MWCNTs/SPCE (c') toward phosphate buffer (pH 7.0) containing 50 μM DA. Curve (d) represents the CV obtained at Au NRs@*f*-MWCNTs/SPCE in phosphate buffer (pH 7.0) in absence of DA. The potential range was − 0.2 V to 0.6 V and the scan rate was 50 mV s^{-1}. Both unmodified SPCE and *f*-MWCNTs/SPCE are shown feeble irreversible peak toward electrocatalytic oxidation of DA at large overpotential. Interestingly, the voltammogram of Au NRs@*f*-MWCNTs/SPCE displayed highly enhanced quasi-reversible redox peaks for DA electrocatalysis. The formal potential ($E^{\circ\prime}$) of redox couple is + 0.18 V (vs. Ag/AgCl) and the peak potential separation (ΔE_p) value was 23 mV.

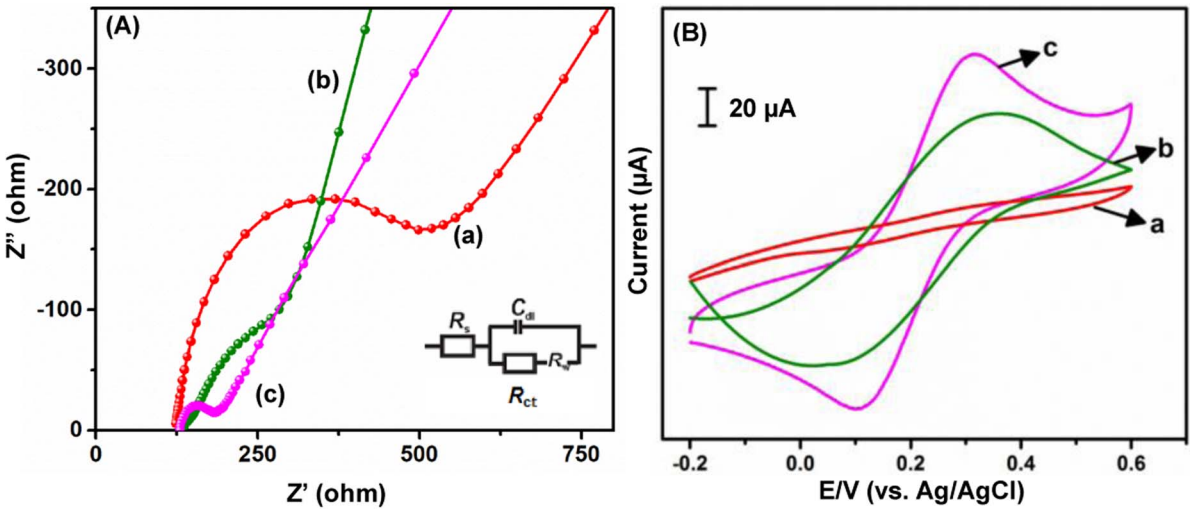

Figure 4. (A) EIS spectra of bare SPCE (a), *f*-MWCNTs/SPCE (b) and Au NRs@f-MWCNTs/SPCE (c) Inset: Randles equivalent circuit model, R_s = electrolyte resistance, R_{ct} = charge transfer resistance C_{dl} = double layer capacitance and Z_w = Warburg impedance. (B) CVs of bare SPCE (a), *f*-MWCNTs/SPCE (b) and Au NRs@f-MWCNTs/SPCE (c) in 0.1 M KCl+5 mM $[Fe(CN)_6]^{3-/4-}$ at scan rate of 50 mVs^{-1}.

Remarkably, the ΔE_p is much lower than the expected value based on Nernst equation, indicating rapid electron transfer of DA electrocatalysis. Due to its excellent electronic properties, the Au NRs@*f*-MWCNTs significantly increases the electron transport at the electrode-electrolyte interface that stands for the observed low ΔE_p. In addition, the redox peak currents, particularly oxidation peak current is much sharper and it is about five fold larger than the peak current observed at *f*-MWCNTs, indicates synergic effect. At the nanocomposite modified electrode, the overpotential of DA oxidation is significantly minimized compared to *f*-MWCNTs, which indicate its good electrocatalytic ability. Thus, the Au NRs@*f*-MWCNTs composite able to catalyze the DA electron transfer as well as greatly amplifies the current signal, suggesting this composite can be a suitable material to develop sensitive DA sensor.

Figure 5b portrays the CVs of Au NRs@*f*-MWCNTs/SPCE toward different concentrations of DA. The DA redox peak currents are linearly increased as the concentration increases from (inset to Figure 5b). The effect of scan rate toward electrocatalysis of DA at Au NRs@*f*-MWCNTs/SPCE was analyzed. As shown in Figure S3a, the peak current increases and as the scan rate increases. In addition, the anodic peak was shifted toward positive potential, while the cathodic peak was shifted toward more negative potential region. The plot of peak currents versus square root of scan rate is exhibited good linearity ($R^2 = 0.990$), suggesting the diffusion controlled DA electrocatalysis at the modified electrode (Figure S3b).

Figure 5c represents the voltammograms obtained at Au NRs@*f*-MWCNTs/SPCE toward 50 μM DA in different pH. A stable quasi-reversible redox couple was observed under all pH conditions, however the values of formal potential (E°') and peak currents were varied. Both anodic (E_{pa}) and cathodic peak potentials (E_{pc}) are shifted toward negative direction as pH increases from 3 to 11. The regression plot between E°' and pH exhibited good linearly and the slope was obtained as 58.8 (±0.12) mV/pH (inset a', Figure 5c). This slope value is in close agreement with the theoretical standard value of −58.6 mV/pH calculated from a Nernst equation for a reversible reaction involving equal numbers of protons and electrons. This result is in accordance with well-established two electrons and two protons coupled redox process of DA at electrode surfaces. Maximum peak current was observed when pH was 7.0 (inset b', Figure 5c); therefore, we use this pH as optimized pH to fabricate DA sensor using our modified electrode.

Amperometric determination of DA.—Figure 6a displays amperometric response of Au NRs@*f*-MWCNTs film modified electrode upon successive injections of DA into phosphate buffer (pH 7.0) at regular intervals of 50 s. The electrode potential was + 0.12 V (vs. Ag/AgCl) and the electrode rotation speed was 1200 rpm. Sharp and rapid responses were obtained for each injection of DA into the electrolyte solution. The steady-state current has been attained in 5–6s. The plot between response current and concentration of DA displays good linearity. The linear regression equation of the plot was, I (μA) = 0.283 [DA]/μM + 7.6 (Figure 6b). The linear range was 3.5 nM–1550 μM and the sensitivity was 4.04 (±0.58) $\mu A.\mu M^{-1}.cm^{-2}$. The limit of detection (LOD) was calculated to be 5.0×10^{-10} (±0.82) M and the limit of quantification (LOQ) was calculated 16.6×10^{-10} (±1.2) M. The LOD of the sensor was calculated by using the formula, LOD = 3 s_b/S (where, s_b = standard deviation of blank signals and S = sensitivity). As shown in Figure 6c, the amperometric responses of Au NRs@*f*-MWCNTs/SPCE was significantly better than the amperometric performance of unmodified SPCE and *f*-MWCNTs toward sensing DA. The linear range, LOD and sensitivity values are compared with existing DA sensors in a Table I. As displayed in table, the Au NRs@*f*-MWCNTs film modified electrode displayed either comparable or superior performance over previous modifiers. Remarkably, the ability of the material to detect picomolar concentration of DA is useful in order to establish ultrasensitive DA sensors.

Selectivity, storage stability, and reproducibility.—Selectivity of the electrode to detect DA in presence of interfering species such as, folic acid, uric acid, ascorbic acid, glucose, epinephrine, norepinephrine, and H_2O_2. Amperometry responses of the modified electrode toward 25 μM of DA and 250 μM of interferents are tested. The results are represented as relative current responses of the interferents with respect to DA response current (Figure 7a). Here, DA delivered significant current response, while all other tested compounds are shown negligible current responses, indicating selectivity of the electrode toward DA over other compounds. The π stacking interaction between *f*-MWNCTs and phenyl moiety of DA is one of the possible explanations for its selectivity. Although, some of the other species exhibit responses at high overpotential region (> 0.30 V, vs. Ag/AgCl) they produce negligible responses at + 0.12 V (vs. Ag/AgCl). Here, the operating electrode potential is away from the interferences causing high positive potential region, which is due to the modification of Au NRs@*f*-MWCNTs on SPCE surface.

In order to test durability of the sensor, to find out the storage stability of the electrode. The amperometric sensing response of Au NRs@*f*-MWCNTs film modified electrode was monitored

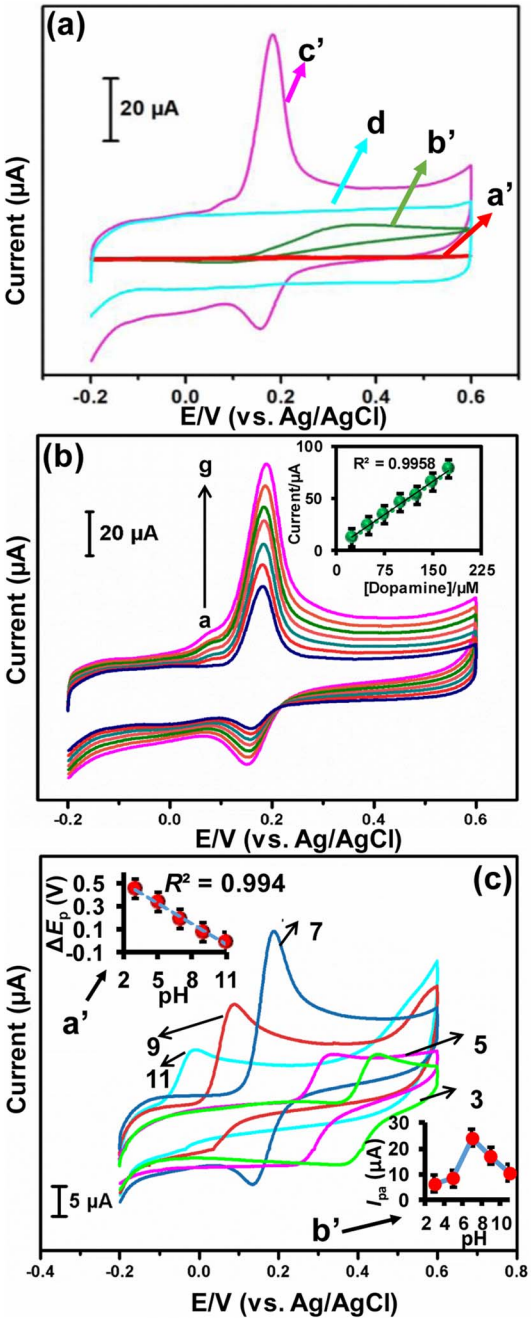

Figure 5. (a) CVs obtained at unmodified (a′), *f*-MWCNTs/SPCE (b′), and Au NRs@*f*-MWCNTs/SPCE (c′) in phosphate buffer (pH 7.0) containing 50 μM DA, and (d) CV obtained at Au NRs@*f*-MWCNTs/SPCE in phosphate buffer (pH 7.0) in absence of DA. (b) CVs obtained at Au NRs@*f*-MWCNTs/SPCE in phosphate buffer (pH 7.0) containing different concentrations of DA (a = 25, b = 50, c = 75, d = 100, e = 125, f = 150 and g = 175 μM), Inset: linear regression plot between peak current (μA) vs. [DA]/μM. (c) CVs obtained at Au NRs@*f*-MWCNTs/SPCE in supporting electrolyte of different pH containing 50 μM DA. Inset (a′) plot between formal potential vs. pH, inset b′: anodic peak current (I_{pa}) (μA) vs. pH.

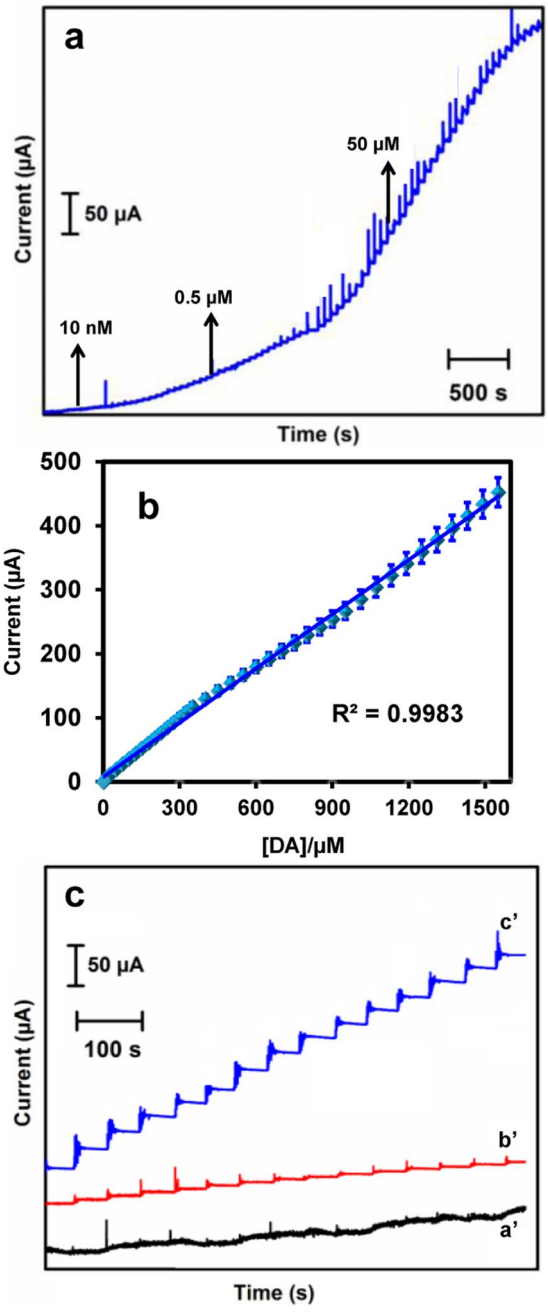

Figure 6. (a) Amperometric response of Au NRs@*f*-MWCNTs film modified electrode for each sequential addition of DA into phosphate buffer (pH 7.0). Electrode rotation speed = 1200 rpm and applied potential = + 0.12 V (vs. Ag/AgCl). (b) Amperometric current (μA) vs. [DA] (μM). (c) Amperometric responses of unmodified (a′), *f*-MWCNTs (b′), Au NRs@*f*-MWCNTs (c′) films modified SPCEs toward different concentrations of DA.

every day, while the electrode was stored at 4°C when not in use. The modified electrode retained 97.05% of its initial current even after 10 days of its continuous use, which endorsed excellent durability (Figure 7b). For the reproducibility studies, measurements at five individual electrodes were recorded in phosphate buffer (pH 7.0) toward 25 μM DA and the R.S.D. was 3.24%. In order to calculate repeatability, five repeated measurements were performed at one modified electrode, and the R.S.D was 3.75%. The results of sensor have acceptable range of repeatability and reproducibility.

Real sample analysis.—To evaluate practicality of the sensor, the Au NRs@*f*-MWCNTs nanocomposite modified SPCE was used to determine DA in human serum and rat brain samples. The human serum and rat brain samples were diluted with 0.1 M phosphate buffer (pH 7.0) in 1:10 ratio before analysis. Known amounts of DA were spiked into the DA free diluted real sample solution. These DA spiked real samples are analyzed using Au NRs@*f*-MWCNTs film

Table I. Comparison of analytical parameters for the detection of DA at Au NRs@*f*-MWCNTs nanocomposite modified electrode with reported works.

Modified Electrode	Linear Range (μM)	LOD (μM)	Ref.
Chitosan/graphene	1.0–24	1.0	25
[a]Au NPs/[b]p-BDD	0.1–0.001	0.06	26
[c]rGO/Bi_2S_3 nanorods	0.01–40	0.0123	27
Ionic liquid-MWCNT/Au NPs	0.08–200	0.03	28
carbon dots-Au nanoclusters	0.005–0.18	0.0029	29
CNT/polyethyleneimine/Au NPs	0.05–4.0	0.0065	30
graphene foam/CNTs/Au NPs	0.10–48	0.0013	31
N-doped MWCNTs/Au NPs	12–322	0.3	32
Graphene/CNTs/MoS_2	0.1–100	0.05	5
graphene/MWCNT/Au	2–213	0.67	33
graphene	4 –100	2.64	34
[d]PDMA-MWCNT/Au NPs	1–100	0.316	35
single-walled carbon nanotubes	1 –10	0.790	36
Au NPs/MoS_2	0.05–30	0.05	37
Au NRs@*f*-MWCNTs	3.5–1550	0.0005	This work

[a]Au NPs = Au nanoparticles.
[b]p-BDD = porous boron-doped diamond.
[c]rGO = reduced graphene oxide.
[d]PDMA = poly diallymethylammonium.

modified SPCE, while the amperometric experimental conditions are same as lab sample experimental conditions. The obtained amperometric curves are given in Figure S4a and S4b. The nanocomposite modified electrode revealed well-defined amperometric responses for each addition of DA from spiked human serum as well as ran brain samples. The linear regression equation clearly reveals the amperometric current are linearly increased with concentration of DA (Figure S4a′ and S4b′). In addition, the found and recoveries for 5 μM and 10 μM concentrations of DA are calculated using standard addition method and given as Table II. As can be seen from table, the sensor retains the recovery ranges of 95.2–98.2% with acceptable relative standard deviation from three independent measurements.

Next, the method was applied in the determination of DA in dopamine hydrochloride injection. Aliquots (10 μL) of dopamine hydrochloride injection solution were injected into phosphate buffer (pH 7.0) and detected via amperometry. The electrode quickly senses the amount of DA present in each aliquots of the injection sample. Moreover, the electrode shows linear sensing performance as displayed in Figure S4c′. The added, found and recovery values are given in Table II and the results are compared with HPLC analysis. The recoveries are in the acceptable range and matched with the HPLC results. From the figure and table, we inferred that the Au NRs@*f*-MWCNTs modified electrode has good capability to sense DA present in dopamine hydrochloride injection.

Conclusions

A highly sensitive, selective and robust electrochemical DA detection platform was developed using Au NRs@*f*-MWCNTs nanocomposite modified electrode, which was prepared by a solution-phase self-assembly approach. Characterization studies confirmed the successful formation of Au NRs and Au NRs@*f*-MWCNTs nanocomposite. However, the material synthesis involves multiple steps. The Au NRs@*f*-MWCNTs nanocomposite modified SPCE displayed greatly improved electrocatalytic activity and lower redox potentials toward DA electrocatalysis than control electrodes. The fabricated

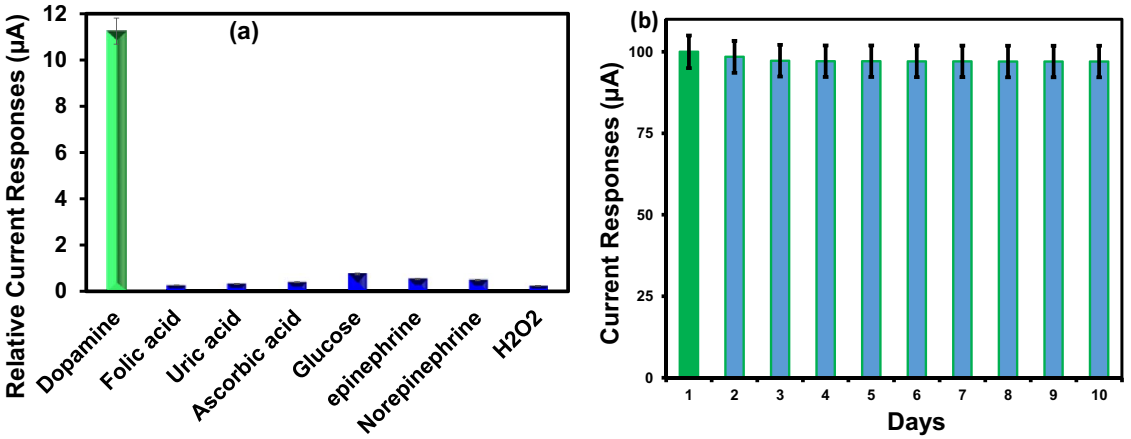

Figure 7. (a) Amperometric response of Au NRs@*f*-MWCNTs film modified electrode toward 25 μM of DA and 250 μM of other interferents. (b) Storage stability: Amperometric sensing performance of Au NRs@*f*-MWCNTs/SPCE toward 25 μM DA.

Table II. Determination of DA in human serum, rat brain and dopamine injection samples Au NRs@*f*-MWCNTs modified electrode, compare with HPLC method.

Samples	Added (μM)	Found (μM)*	Recovery (%)*	Found (μM)#	Recovery (%)#
Human serum	0	0	–	0	–
	5	4.91	98.2	4.98	99.6
	10	9.74	97.4	9.88	98.8
Rat brain	0	0	–	0	–
	5	4.76	95.2	4.94	98.8
	10	9.81	98.1	9.92	99.2
Dopamine injection	0	0.26	-	0.28	-
	5	5.16	103.2	5.19	103.8
	10	10.29	102.9	10.27	102.7

*Detected by Au NRs@*f*-MWCNTs composite modified electrode by amperometry (n = 3).
#Detected by Waters Alliance, model 2695 HPLC (Empower, version 3).

amperometric DA sensor exhibited superior electroanalytical parameters such as wide linear range, low detection limit and good sensitivity toward than previously reported DA sensors. The good recoveries obtained in spiked DA analyses in real samples, indicates practical applicability of the method.

Acknowledgments

The authors extend their appreciation to the International Scientific Partnership Program ISPP at King Saud University for funding this research work through ISPP# 124. This work was supported by the Ministry of Science and Technology, Taiwan (MOST 106-2113-M-027-003).

ORCID

Shen-Ming Chen https://orcid.org/0000-0002-3749-1224

References

1. S. Demuru, L. Nela, N. Marchack, S. J. Holmes, D. B. Farmer, G. S. Tulevski, Q. Lin, and H. Deligianni, *ACS Sensors*, (2018).
2. W. Cai, T. Lai, H. Du, and J. Ye, *Sensors and Actuators B: Chemical*, **193**, 492 (2014).
3. H. Bagheri, A. Afkhami, P. Hashemi, and M. Ghanei, *RSC Advances*, **5**, 21659 (2015).
4. H. Bagheri, N. Pajooheshpour, B. Jamali, S. Amidi, A. Hajian, and H. Khoshsafar, *Microchemical Journal*, **131**, 120 (2017).
5. K. Jackowska and P. Krysinski, *Analytical and bioanalytical chemistry*, **405**, 3753 (2013).
6. R. Devasenathipathy, V. Mani, S.-M. Chen, B. Viswanath, V. Vasantha, and M. Govindasamy, *RSC Advances*, **4**, 55900 (2014).
7. V. Mani, M. Govindasamy, S.-M. Chen, R. Karthik, and S.-T. Huang, *Microchimica Acta*, **183**, 2267 (2016).
8. H. Bagheri, H. Khoshsafar, S. Amidi, and Y. H. Ardakani, *Analytical Methods*, **8**, 3383 (2016).
9. M. Govindasamy, U. Rajaji, S.-M. Chen, S. Kumaravel, T.-W. Chen, F. M. Al-Hemaid, M. A. Ali, and M. S. Elshikh, *Analytica Chimica Acta*, (2018).
10. M. Trojanowicz, *TrAC Trends in Analytical Chemistry*, **25**, 480 (2006).
11. M. Govindasamy, S.-M. Chen, V. Mani, R. Devasenathipathy, R. Umamaheswari, K. J. Santhanaraj, and A. Sathiyan, *Journal of colloid and interface science*, **485**, 129 (2017).
12. B. Unnikrishnan, V. Mani, and S.-M. Chen, *Sensors and Actuators B: Chemical*, **173**, 274 (2012).
13. M. Govindasamy, V. Mani, S.-M. Chen, R. Karthik, K. Manibalan, and R. Umamaheswari, *Int. J. Electrochem. Sci*, **11**, 2954 (2016).
14. G. G. Wildgoose, C. E. Banks, and R. G. Compton, *Small*, **2**, 182 (2006).
15. V. Mani, M. Govindasamy, S.-M. Chen, T.-W. Chen, A. S. Kumar, and S.-T. Huang, *Scientific reports*, **7**, 11910 (2017).
16. R. Devasenathipathy, C. Karuppiah, S.-M. Chen, V. Mani, V. S. Vasantha, and S. Ramaraj, *Microchimica Acta*, 1 (2014).
17. R. Devasenathipathy, V. Mani, S.-M. Chen, D. Arulraj, and V. Vasantha, *Electrochimica Acta*, **135**, 260 (2014).
18. V. K. Ponnusamy, V. Mani, S.-M. Chen, W.-T. Huang, and J.-F. Jen, *Talanta*, **120**, 148 (2014).
19. Q.-L. Zhang, J.-X. Feng, A.-J. Wang, J. Wei, Z.-Y. Lv, and J.-J. Feng, *Microchimica Acta*, **182**, 589 (2015).
20. W. Lu, G. Zhang, R. Zhang, L. G. Flores, Q. Huang, J. G. Gelovani, and C. Li, *Cancer research*, **70**, 3177 (2010).
21. M. N. Karim, J. E. Lee, and H. J. Lee, *Biosensors and Bioelectronics*, **61**, 147 (2014).
22. B. Su, J. Tang, H. Yang, G. Chen, J. Huang, and D. Tang, *Electroanalysis*, **23**, 832 (2011).
23. M. Alagiri, P. Rameshkumar, and A. Pandikumar, *Microchimica Acta*, **184**, 3069 (2017).
24. N. Yusoff, A. Pandikumar, R. Ramaraj, H. N. Lim, and N. M. Huang, *Microchimica Acta*, **182**, 2091 (2015).
25. Q. Zhu, J. Wu, J. Zhao, and W. Ni, *Langmuir*, **31**, 4072 (2015).
26. C.-S. Dai, P.-Y. Chien, J.-Y. Lin, S.-W. Chou, W.-K. Wu, P.-H. Li, K.-Y. Wu, and T.-W. Lin, *ACS applied materials & interfaces*, **5**, 12168 (2013).
27. M. Govindasamy, V. Mani, S.-M. Chen, T. Maiyalagan, S. Selvaraj, T.-W. Chen, S.-Y. Lee, and W.-H. Chang, *RSC Advances*, **7**, 33043 (2017).
28. W. Haiss, N. T. Thanh, J. Aveyard, and D. G. Fernig, *Analytical chemistry*, **79**, 4215 (2007).
29. B. Kim and W. M. Sigmund, *Langmuir*, **20**, 8239 (2004).
30. Z. Xing, Z. Ju, Y. Zhao, J. Wan, Y. Zhu, Y. Qiang, and Y. Qian, *Scientific reports*, **6**, 26146 (2016).
31. S. K. Movahed, M. Fakharian, M. Dabiri, and A. Bazgir, *Rsc Advances*, **4**, 5243 (2014).
32. H. Bagheri, E. Ranjbari, M. Amiri-Aref, A. Hajian, Y. H. Ardakani, and S. Amidi, *Biosensors and Bioelectronics*, **85**, 814 (2016).
33. H. Bagheri, A. Afkhami, H. Khoshsafar, A. Hajian, and A. Shahriyari, *Biosensors and Bioelectronics*, **89**, 829 (2017).
34. T. Rahmani, A. Hajian, A. Afkhami, and H. Bagheri, *New Journal of Chemistry*, **42**, 7213 (2018).
35. H. Bagheri, H. Khoshsafar, A. Afkhami, and S. Amidi, *New Journal of Chemistry*, **40**, 7102 (2016).